

X-ray-absorption and -emission spectra of a K_2PdCl_6 crystal studied by the self-consistent-charge extended Hückel method

Michihide Kitamura, Chikara Sugiura, and Shinji Muramatsu
 Department of Electrical and Electronic Engineering, Faculty of Engineering,
 Utsunomiya University, Utsunomiya 321, Japan
 (Received 14 November 1988)

Molecular-orbital calculations are performed for an octahedral complex $(PdCl_6)^{2-}$ with a self-consistent-charge extended Hückel method and used to analyze experimental x-ray-absorption and -emission spectra for K_2PdCl_6 crystals. Our calculations are entirely based on first principles in the sense that empirical atomic data are not used. The observed features for the x-ray-absorption and -emission spectra are shown to be generally accounted for by our calculations.

I. INTRODUCTION

For the purpose of obtaining information on electronic structures, we investigate x-ray-absorption and -emission spectra for K_2PdCl_6 experimentally and theoretically, focusing our attention on both a central Pd and its ligand Cl ions, which form an octahedral complex $(PdCl_6)^{2-}$ in K_2PdCl_6 crystal. It is fundamentally sound to study the electronic structures for such a complex in terms of the molecular-orbital (MO) theory.¹⁻⁹ On the experimental side, we have measured the Pd $L\beta_{2,15}$ and Cl $K\beta$ emission spectra to compare them with the Pd L_{III} and Cl K absorption spectra reported previously.^{10,11} From the theoretical side, we make an attempt to analyze the experimental results on both the absorption and emission from a MO approach based on a self-consistent-charge extended Hückel method, which has been successfully used for transition-metal compounds^{2,6,7} and for some xenon, thorium, and uranium fluorides.^{8,9}

It should be pointed out that in 1970 Fischer extensively studied electronic structures from the x-ray spectra in terms of the MO theory.¹² He used the x-ray spectra to empirically deduce the complete molecular-orbital arrangement of various compounds and showed that a MO model is very effective in interpreting the x-ray experimental results.

We have so far studied the x-ray-absorption near-edge structure (XANES) for several materials on the basis of multiple-scattering theory and substantiated that this theory is adequate for a description of the x-ray-absorption process.¹³⁻¹⁸ However, in this paper we are interested in understanding both the absorption and emission spectra. The MO theory can be used to describe the overlapping spectral regions for the absorption and emission spectra, and it is expected that useful information can be extracted from a comparison of the experimental x-ray spectra involving both absorption and emission with theoretical ones based on the MO theory. In our molecular-orbital calculations, we do not use empirical atomic data. Starting from first principles, we perform molecular-orbital calculations. Our approach to realize this spirit is similar to that employed by Larsson

*et al.*⁸ and by Larsson and Pyykkö.⁹

The K_2PdCl_6 crystal can be regarded as $K_2^+Q^{2-}$ ($Q = PdCl_6$), and the $K_2^+Q^{2-}$ has the CaF_2 -type arrangement. In the calculation of the electronic structure for the complex consisting of a central Pd metal and six ligand Cl ions, we have considered only the charge transfer between Pd and Cl ions within the complex Q , assuming that the charges on the K and complex Q are +1 and -2. Here, we should briefly describe the crystal structure of K_2PdCl_6 , which is necessary in the course of our calculations. The Q^{2-} ions are located on the eight corners and on the six face centers of the cube of a unit cell shown in Fig. 1, while the K^+ ions are located on the following positions: $a_0(\frac{1}{4}, \frac{1}{4}, \frac{1}{4})$, $a_0(\frac{3}{4}, \frac{1}{4}, \frac{1}{4})$, $a_0(\frac{3}{4}, \frac{3}{4}, \frac{1}{4})$, $a_0(\frac{1}{4}, \frac{3}{4}, \frac{1}{4})$, $a_0(\frac{1}{4}, \frac{1}{4}, \frac{3}{4})$, $a_0(\frac{3}{4}, \frac{1}{4}, \frac{3}{4})$, $a_0(\frac{3}{4}, \frac{3}{4}, \frac{3}{4})$, and $a_0(\frac{1}{4}, \frac{3}{4}, \frac{3}{4})$, where a_0 is the lattice constant, having the value of 9.74 Å.¹⁹ The complex Q^{2-} forms an octahed-

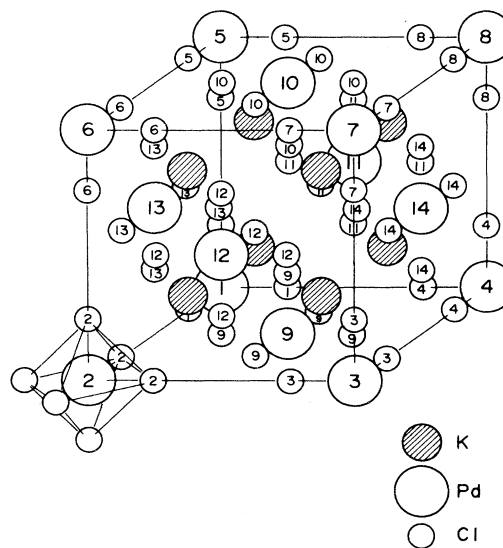


FIG. 1. Unit cell of K_2PdCl_6 crystal. An octahedron is also illustrated.

ron. The distance between Pd and Cl ions, which corresponds to the value of u in the table of Wyckoff,¹⁹ is not known for K_2PdCl_6 . However, the u value for several other crystals having the same crystal structure is known as ~ 0.24 , and it is 0.243 for K_2OsCl_6 ,¹⁹ which has a lattice constant (9.729 Å) very close to that of K_2PdCl_6 . We chose 0.243 as the value of u for K_2PdCl_6 .

II. EXPERIMENT

The specimen of K_2PdCl_6 under study was purchased from the Kanto Chemical Company (Japan), was in fine powder form, and was of 99.9% purity. The palladium $L\beta_{2,15}$ and chlorine $K\beta$ emission spectra in fluorescence were measured with a Rigaku two-crystal vacuum spectrometer²⁰ with Si(111) crystals at the temperature of 36.5°C, which was stabilized within $\pm 0.5^\circ\text{C}$ during the measurement. The fluorescent x-ray emitter of the compound was prepared by uniformly rubbing its fine powder onto a sheet of paper. A chromium target x-ray tube was operated at 50 kV and 50 mA as a primary x-ray source. In this procedure, the palladium $L\beta_{2,15}$ and chlorine $K\beta$ emission spectra were mainly excited by the Cr $K\alpha$ emission ($K\alpha_1$, 5414.7 eV). The intensity measurements were carried out automatically for a preset counting time at regular intervals of 0.005° in the Bragg angle by means of a step-scanning method. The detector was a gas-flow proportional counter equipped with a thin polypropylene window, using argon gas with 10% methane by volume. The present spectra have been obtained by averaging ten runs. The metallic Pd $L\beta_{2,15}$ line (3171.79 eV) (Ref. 21) and the sharp Cl $K\beta_1$ line (2815.17 eV) (Ref. 22) of KCl were used as reference lines to determine the photon-energy values of the Pd $L\beta_{2,15}$ and Cl $K\beta$ emission spectra of K_2PdCl_6 .

The Cl K (Ref. 10) and Pd L_{III} (Ref. 11) absorption spectra for K_2PdCl_6 crystal have been already measured by using a 50-cm-radius bent-quartz-crystal vacuum spectrograph of the Johann type. Details of the absorption measurements are described in these papers.^{10,11}

III. THEORETICAL DETAILS

We consider the electronic structure of an octahedral cluster MX_6 shown in Fig. 2, where a metal (M) atom (or ion) is denoted by 0 and six ligand (X) atoms (or ions) are denoted by α ($\alpha=1,2,\dots,6$). The eigenfunctions of the system are classified according to the irreducible representations of O_h symmetry. The molecular orbital (MO) $\Psi(\Gamma;\gamma)$ belonging to the irreducible representation Γ and its component γ ($\gamma=1,2,\dots,g_\Gamma$) is represented as

$$\Psi(\Gamma;\gamma) = \sum_i u_i \psi(\Gamma;\gamma)_i, \quad (1)$$

where the $\psi(\Gamma;\gamma)_i$'s include atomic orbitals of the metals and symmetry-adopted normalized combination of ligand atomic orbitals. The subscript i is used to differentiate among $\psi(\Gamma;\gamma)$'s with the same $(\Gamma;\gamma)$. Adopting s , p , and d atomic orbitals ($s^{(0)}$, $p^{(0)}$, and $d^{(0)}$) for Pd metal and s and p ones ($s^{(\alpha)}$ and $p^{(\alpha)}$) for Cl ligands, $\Psi(\Gamma;\gamma)$ in (1) is explicitly written as follows:

$$\Psi(a_{1g}) = u_1 s^{(0)} + u_2 \psi(a_{1g}, s) + u_3 \psi(a_{1g}, p\sigma), \quad (2a)$$

$$\begin{aligned} \Psi(t_{1u}; \gamma) &= u_1 p_\gamma^{(0)} + u_2 \psi(t_{1u}; \gamma, s) + u_3 \psi(t_{1u}; \gamma, p\sigma) \\ &\quad + u_4 \psi(t_{1u}; \gamma, p\pi) \\ (p_1^{(0)} \equiv p_x^{(0)}, p_2^{(0)} \equiv p_y^{(0)}, p_3^{(0)} \equiv p_z^{(0)}), \end{aligned} \quad (2b)$$

$$\begin{aligned} \Psi(e_g; \gamma) &= u_1 d_\gamma^{(0)} + u_2 \psi(e_g; \gamma, s) + u_3 \psi(e_g; \gamma, p\sigma), \\ (d_1^{(0)} \equiv d_{z^2}^{(0)}, d_2^{(0)} \equiv d_{x^2-y^2}^{(0)}), \end{aligned} \quad (2c)$$

$$\begin{aligned} \Psi(t_{2g}; \gamma) &= u_1 d_\gamma^{(0)} + u_2 \psi(t_{2g}; \gamma, p\pi), \\ (d_1^{(0)} \equiv d_{yz}^{(0)}, d_2^{(0)} \equiv d_{zx}^{(0)}, d_3^{(0)} \equiv d_{xy}^{(0)}), \end{aligned} \quad (2d)$$

$$\Psi(t_{1g}; \gamma) = \psi(t_{1g}; \gamma, p\pi), \quad (2e)$$

$$\Psi(t_{2u}; \gamma) = \psi(t_{2u}; \gamma, p\pi). \quad (2f)$$

Here, $\psi(\Gamma;\gamma,\lambda)$ ($\lambda=s, p\sigma$, and $p\pi$) is the so-called group orbital belonging to the $\Gamma(\gamma)$, whose expression is given in Ref. 2.

The coefficients $u_i(\Gamma)$ and eigenvalues $E(\Gamma)$ are obtained by solving the following equation iteratively until a self-consistent charge is attained:

$$\mathbf{H}(\Gamma)\mathbf{u}(\Gamma) = \mathbf{S}(\Gamma)\mathbf{u}(\Gamma)E(\Gamma), \quad (3a)$$

where

$$H_{ij}(\Gamma) = \langle \psi(\Gamma)_i | \mathbf{H} | \psi(\Gamma)_j \rangle, \quad (3b)$$

$$S_{ij}(\Gamma) = \langle \psi(\Gamma)_i | \psi(\Gamma)_j \rangle. \quad (3c)$$

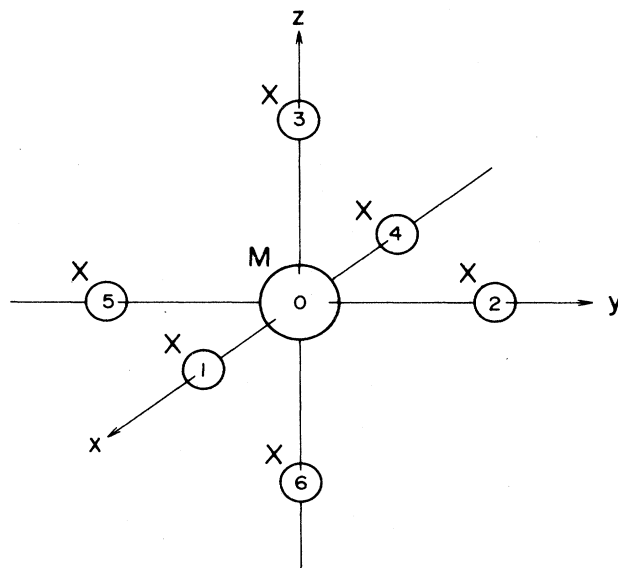


FIG. 2. An octahedron MX_6 . Site members (0-6) are indicated.

We must evaluate the matrix elements for \mathbf{H} , which indicates a one-electron Hamiltonian. In the following, we will show how the matrix elements and the overlap integral S_{ij} can be expressed in terms of atomic quantities, taking the case of $\Gamma = t_{2g}$ as an example.

For the case of $\Gamma = t_{2g}$ and $\gamma = 3$, the MO $\Psi(t_{2g}; 3)$ and the group orbital $\psi(t_{2g}; 3, p\pi)$ are given by

$$\Psi(t_{2g}; 3) = u_1 d_{xy}^{(0)} + u_2 \psi(t_{2g}; 3, p\pi), \quad (4a)$$

$$\psi(t_{2g}; 3, p\pi) = N(t_{2g}; 3, p\pi)(p_x^{(2)} - p_x^{(5)} + p_y^{(1)} - p_y^{(4)}), \quad (4b)$$

where

$$H_{11} = E_d^{(M)}, \quad (5a)$$

$$H_{22} = N(t_{2g}; 3, p\pi)^2 (E_p^{(x)} - \langle p_x^{(2)} | \mathbf{H} | p_x^{(5)} \rangle + \langle p_x^{(2)} | \mathbf{H} | p_y^{(1)} \rangle - \langle p_x^{(2)} | \mathbf{H} | p_y^{(4)} \rangle - \langle p_x^{(5)} | \mathbf{H} | p_x^{(2)} \rangle + E_p^{(x)} - \langle p_x^{(5)} | \mathbf{H} | p_y^{(1)} \rangle + \langle p_x^{(5)} | \mathbf{H} | p_y^{(4)} \rangle + \langle p_y^{(1)} | \mathbf{H} | p_x^{(2)} \rangle - \langle p_y^{(1)} | \mathbf{H} | p_x^{(5)} \rangle + E_p^{(x)} - \langle p_y^{(1)} | \mathbf{H} | p_y^{(4)} \rangle - \langle p_y^{(4)} | \mathbf{H} | p_x^{(2)} \rangle + \langle p_y^{(4)} | \mathbf{H} | p_x^{(5)} \rangle - \langle p_y^{(4)} | \mathbf{H} | p_y^{(1)} \rangle + E_p^{(x)}), \quad (5b)$$

$$H_{12} = H_{21}^* = N(t_{2g}; 3, p\pi) (\langle d_{xy}^{(0)} | \mathbf{H} | p_x^{(2)} \rangle - \langle d_{xy}^{(0)} | \mathbf{H} | p_x^{(5)} \rangle + \langle d_{xy}^{(0)} | \mathbf{H} | p_y^{(1)} \rangle - \langle d_{xy}^{(0)} | \mathbf{H} | p_y^{(4)} \rangle), \quad (5c)$$

where $E_d^{(M)}$ and $E_p^{(X)}$ are the energies of d and p atomic orbitals, respectively, containing a Madelung correction at M and X sites. We calculate the Madelung correction with Evjen's method²³ at every step of iterations for self-consistency of the charge, taking into account ligand-to-metal charge transfer. In the evaluation for the matrix elements of \mathbf{H} between atomic orbitals such as $\langle p_x^{(2)} | \mathbf{H} | p_x^{(5)} \rangle$ and $\langle d_{xy}^{(0)} | \mathbf{H} | p_x^{(2)} \rangle$ appearing in (5b) and (5c), we use the Wolfsberg-Helmholtz approximation,²⁴

$$\langle p_x^{(2)} | \mathbf{H} | p_x^{(5)} \rangle = G(E_p^{(X)} + E_p^{(X)}) \langle p_x^{(2)} | p_x^{(5)} \rangle / 2$$

and

$$\langle d_{xy}^{(0)} | \mathbf{H} | p_x^{(2)} \rangle = G(E_d^{(M)} + E_p^{(X)}) \langle d_{xy}^{(0)} | p_x^{(2)} \rangle / 2,$$

where G is an adjustable parameter. Thus, the quantities needed to solve Eq. (3a) are all expressed in terms of the atomic energies corrected by the Madelung term including the charge transfer and the overlap integrals (Δ) between atomic orbitals on the different atoms at \mathbf{r}_α and \mathbf{r}_β . These general overlap integrals can be transformed into basic overlap integrals such as $\Delta_{pp\sigma}$ and $\Delta_{pp\pi}$ by use of the direction cosines (l, m, n) of $\mathbf{r}_\beta - \mathbf{r}_\alpha$, as shown in the table of Slater and Koster.²⁵ Here, $\Delta_{pp\sigma}$ and $\Delta_{pp\pi}$ are the basic overlap integrals between two p orbitals for σ and π states, respectively. For example, $\langle p_x^{(\alpha)} | p_y^{(\beta)} \rangle$ is written as $lm\Delta_{pp\sigma}(|\mathbf{r}_\alpha - \mathbf{r}_\beta|) - lm\Delta_{pp\pi}(|\mathbf{r}_\alpha - \mathbf{r}_\beta|)$. We numerically calculated these integrals by use of elliptic coordinates.²⁶

The intensities $I(\Gamma, nl)$ for absorption and emission are calculated by using the MO $\Psi(\Gamma; \gamma)$ and inner-core orbit-

$$N(t_{2g}; 3, p\pi) = [4 - 2(\langle p_x^{(2)} | p_x^{(5)} \rangle + \langle p_y^{(1)} | p_y^{(4)} \rangle - \langle p_x^{(2)} | p_y^{(1)} \rangle + \langle p_x^{(2)} | p_y^{(4)} \rangle + \langle p_x^{(5)} | p_y^{(1)} \rangle - \langle p_x^{(5)} | p_y^{(4)} \rangle)]^{-1/2}. \quad (4c)$$

The coefficients u_1 and u_2 in (4a) satisfy the following normalization condition:

$$u_1^2 + u_2^2 + u_1 u_2 [\langle d_{xy}^{(0)} | \psi(t_{2g}; 3, p\pi) \rangle + \langle \psi(t_{2g}; 3, p\pi) | d_{xy}^{(0)} \rangle] = 1. \quad (4d)$$

In this case, Eq. (3a) is the 2×2 matrix equation. The matrix elements for (3b) are given as follows:

al $\phi_{nl\rho}^{(\alpha)}$, as follows:

$$I(\Gamma, nl) = \sum_{\alpha} I_{\alpha}(\Gamma, nl). \quad (6)$$

Here, the summation is taken over sites α 's. $I_{\alpha}(\Gamma, nl)$ is written as

$$I_{\alpha}(\Gamma, nl) \propto \int d\hat{\mathbf{e}} \sum_{\rho} \sum_{\gamma} |\langle \phi_{nl\rho}^{(\alpha)} | \mathbf{e} \cdot \mathbf{r} | \Psi(\Gamma; \gamma) \rangle|^2. \quad (7)$$

On the basis of a formula using a spherical harmonic Y_l^m ,

$$\mathbf{e} \cdot \mathbf{r} = (4\pi/3)er \sum_m Y_1^m(\hat{\mathbf{e}}) Y_1^m(\hat{\mathbf{r}}),$$

Eq. (7) is rewritten as

$$I_{\alpha}(\Gamma, nl) \propto \sum_{\rho} \sum_{\gamma} \sum_m |\langle \phi_{nl\rho}^{(\alpha)} | r Y_1^m(\hat{\mathbf{r}}) | \Psi(\Gamma; \gamma) \rangle|^2. \quad (8)$$

For example, the $I(t_{2g}, 2p)$ for $2p \leftrightarrow t_{2g}$ transitions, which contribute to the Pd $L_{II,III}$ absorption or Pd $L\beta_{2,15}$ emission, is given by

$$I(t_{2g}, 2p) \propto 3u_1^2 \left| \int_0^{\infty} r^3 R_{nd}^{(0)}(r) R_{2p}^{(0)}(r) dr \right|^2 \times |\langle Y_2^2 | Y_1^1 | Y_1^1 \rangle|^2, \quad (9)$$

where $\langle Y_3^{m_3} | Y_1^{m_1} | Y_2^{m_2} \rangle$ is a Gaunt integral.¹³ The integral for radial wave functions $R_{nd}^{(0)}$ and $R_{2p}^{(0)}$ is numerically carried out by using these wave functions obtained from the SCF calculations for atoms. We should note that the summation over α in Eq. (6) is taken only for

$\alpha=0$ in the calculation of Pd spectra and for $\alpha=1,2,\dots,6$ in the calculation of Cl spectra. This approximation is only valid when the overlap between metal and ligand orbitals is not large, as shown by Larsson *et al.*⁸ referring to Manne-Åberg theorem.²⁷ Checking the magnitudes of the overlaps, we have confirmed that our approximation can be used in the present calculations.

Next, let us proceed to calculational detail, focusing our attention on a procedure for charge consistency. We have started the iteration for the charge consistency, assuming the electron configurations for Pd and Cl as Pd, $(4d)^{6-x-y+q}(5s)^x(5p)^y$; and Cl, $(3s)^2(3p)^{6-q/6}$, where q denotes the charge transfer from six Cl⁻ ions to the Pd⁴⁺ ion. For instance, x is given by

$$x = \sum'_{\{\Gamma=a_{1g}\}} n(\Gamma) \langle u, s^{(0)} | \Psi(\Gamma; \gamma) \rangle, \quad (10)$$

where $n(\Gamma)$ is the occupation number of electrons on MO $\Psi(\Gamma; \gamma)$ and $\sum'_{\{\Gamma=a_{1g}\}}$ means that the summation is taken for only $\Gamma=a_{1g}$.

The calculation is continued until the output change (x_{out} , y_{out} , and z_{out}) coincides with the input charge (x_{in} , y_{in} , and z_{in}) within a certain tolerance value β :

$$\text{Max}[|x_{out}-x_{in}|, |y_{out}-y_{in}|, |z_{out}-z_{in}|] \leq \beta \quad (11)$$

When Eq. (11) is not satisfied, the calculation is iterated again by taking new input charges given by $(\omega_{in} + \omega_{out})/2$

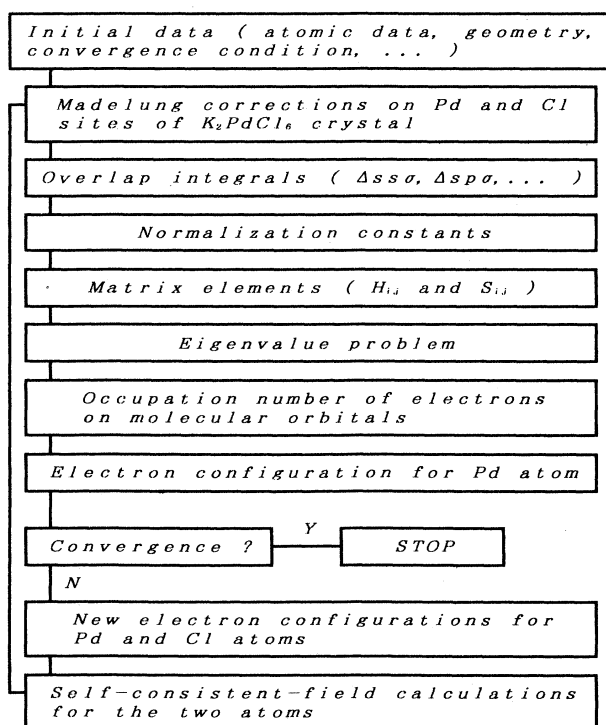


FIG. 3. Flow chart for our calculations based on the self-consistent-charge extended Hückel method.

($\omega=x, y$, and z).

The flow chart for our calculation is shown in Fig. 3. Here, we should emphasize that our self-consistent calculations have been carried out from first principles without using empirical atomic data on the basis of the prescription of Herman and Skillman²⁸ using Schwarz's exchange parameter²⁹ for the atoms.

Finally, we mention the adjustable parameter G . The G value of 1.75 is widely used.^{24,30} Generally speaking, however, it should be a function of the overlap integral (Δ). Cusachs used a overlap-dependent parameter such as $2-|\Delta|$.³¹ In this paper we have done calculations using two types of G : $G=1.75$ and $G=2-|\Delta|$.

IV. RESULTS AND DISCUSSION

A. Result of calculations

The self-consistent charges and electron configurations of Pd and Cl ions are presented in Tables I and II, togeth-

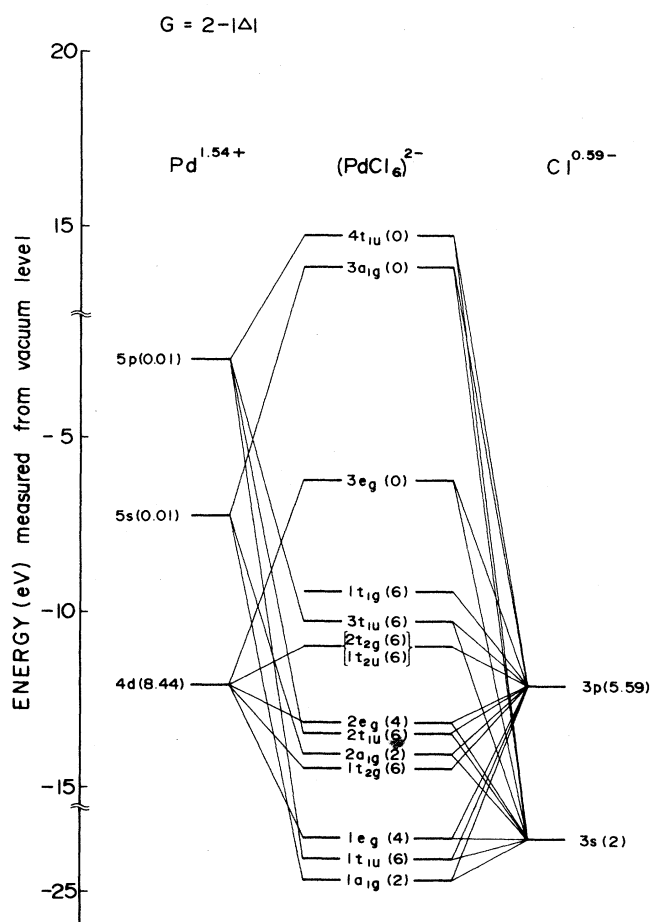


FIG. 4. Energy diagram of the molecular-orbital levels calculated for $G=2-|\Delta|$. Levels for the $4d$, $5s$, and $5p$ atomic orbitals of the Pd ion and for the $3s$ and $3p$ ones of the Cl ion, including the Madelung corrections. The numbers indicated in parentheses are the occupation numbers of electrons on the respective levels.

TABLE I. Results obtained for $G=2-|\Delta|$ on the basis of the self-consistent-charge extended Hückel method within the accuracy of 0.01e. The energies of MO's and atomic orbitals including the Madelung corrections and self-consistent charges are listed along with values of coefficients u_i 's of MO's. The energy is measured from the vacuum level.

Γ	Energy (eV)	$G=2- \Delta $			
		u_1	u_2	u_3	u_4
$4t_{1u}$	14.8	-1.57	-0.762	0.569	0.457
$3a_{1g}$	13.9	1.64	-0.745	0.892	
$3e_g$	-6.16	0.749	0.353	-0.843	
$1t_{1g}$	-9.33	1.00			
$3t_{1u}$	-10.2	-0.113	0.146	-0.816	0.670
$2t_{2g}$	-10.9	0.904	-0.578		
$1t_{2u}$	-10.9	1.00			
$2e_g$	-13.1	0.705	0.118	0.585	
$2t_{1u}$	-13.4	0.103	-0.188	-0.569	-0.813
$2a_{1g}$	-14.0	0.116	0.322	1.07	
$1t_{2g}$	-14.4	0.452	0.829		
$1e_g$	-23.4	0.150	-0.954	-0.0841	
$1t_{1u}$	-24.0	-0.148	-1.04	0.0371	0.218
$1a_{1g}$	-24.6	-0.0187	-0.939	0.178	
$\text{Pd}^{1.54+}(4d^{8.44}5s^{0.01}5p^{0.01}), \text{Cl}^{0.59-}(3s^{2.3}3p^{5.59})$					
	$4d$	$5s$	$5p$	$3s$	$3p$
Energy (eV)	-12.05	-7.243	-2.754	-23.44	-12.04

er with the results for the energies and the coefficients u_i 's of MO's. The self-consistency of the charges is attained within the accuracy of 0.01e. Our result for the self-consistent charges that largely differ from the formal charges ($\text{Pd}^{4+}, \text{Cl}^{-}$) indicates that the $(\text{PdCl}_6)^{2-}$ complex forms highly covalent bonds. Bhat has already found experimentally the high covalency of the Cl ion in K_2PdCl_6 from measurements of the Cl K x-ray-absorption spectra for NaCl, YCl_3 , AuCl_3 , and K_2PdCl_6 .³² The covalencies for the Cl ions in NaCl, YCl_3 , and AuCl_3 are 0%, 20%,

and 40%, respectively. From the measured intensity for the first peaks of these spectra, he deduced that the covalency for the Cl ion in K_2PdCl_6 is larger than that of AuCl_3 . Namely, it is larger than 40%. His result is consistent with ours for the covalency of 40–41% for the Cl ion in K_2PdCl_6 .

The energy diagram of MO levels is shown in Figs. 4 and 5, together with the energy levels for $4d$, $5s$, and $5p$ atomic orbitals of the Pd ion and the $3s$ and $3p$ ones of the Cl ion, which are used as basis functions for a con-

TABLE II. Same as in Table I, but for $G=1.75$.

Γ	Energy (eV)	$G=1.75$			
		u_1	u_2	u_3	u_4
$4t_{1u}$	18.3	-1.57	-0.813	0.565	0.453
$3a_{1g}$	16.4	1.62	-0.749	0.926	
$3e_g$	-7.39	-0.775	-0.307	0.830	
$1t_{1g}$	-10.3	1.00			
$3t_{1u}$	-10.9	-0.0935	0.113	-0.811	0.693
$2t_{2g}$	-11.1	0.943	-0.485		
$1t_{2u}$	-11.6	1.00			
$2e_g$	-13.0	0.683	0.0749	0.607	
$2t_{1u}$	-13.6	0.0916	-0.135	-0.585	-0.795
$2a_{1g}$	-14.2	0.0146	0.284	1.02	
$1t_{2g}$	-14.2	0.360	0.885		
$1e_g$	-23.6	0.100	-0.972	-0.0668	
$1t_{1u}$	-24.1	-0.0550	-1.01	0.0111	0.123
$1a_{1g}$	-24.9	-0.0359	-0.957	0.0967	
$\text{Pd}^{1.60+}(4d^{8.30}5s^{0.06}5p^{0.04}), \text{Cl}^{0.60-}(3s^{2.3}3p^{5.60})$					
	$4d$	$5s$	$5p$	$3s$	$3p$
Energy (eV)	-11.82	-7.056	-2.575	-23.90	-12.41

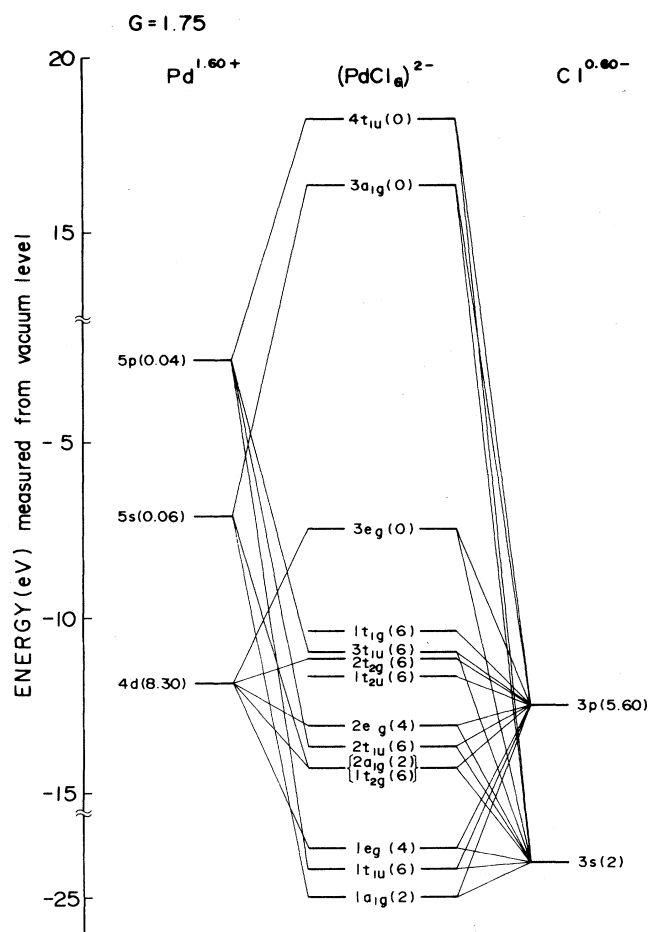


FIG. 5. Same as in Fig. 4, but for $G = 1.75$.

struction of the MO. The energy levels indicated in these figures for the atomic orbitals include the Madelung corrections. The energy separation between $3e_g$ and $2t_{2g}$ MO levels, which is usually called $10Dq$, is 4.74 eV for $G = 2 - |\Delta|$ and 3.71 eV for $G = 1.75$. These values are comparable with the values found for most octahedral complexes;³³ for example, 2.52 eV for $(\text{RhCl}_6)^{3-}$ and 4.23 eV for $[\text{Rh}(\text{NH}_3)_6]^{3+}$.

B. Comparison of experiment and calculation

We have calculated Pd L_{III} absorption and Pd $L\beta_{2,15}$ emission spectra as well as Cl K absorption and Cl $K\beta$ emission spectra using the obtained MO's and their energies given in Tables I and II, to compare theoretical spectra with experimental ones. The measured Pd L_{III} absorption and Pd $L\beta_{2,15}$ emission spectra are shown in Fig. 6, and the measured Cl K absorption and Cl $K\beta$ emission in Fig. 7, together with the calculated spectra. In these figures the absorption spectra are illustrated by dashed curves and the emission spectra by solid curves. From these figures we see that the observed Pd $L\beta_{2,15}$

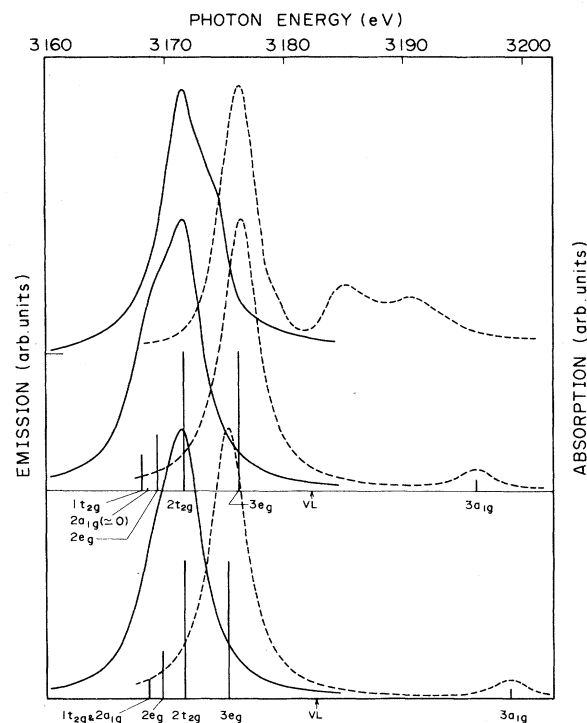


FIG. 6. Pd $L\beta_{2,15}$ emission (solid curves) and Pd L_{III} absorption (dashed curves) spectra. The upper curves are experimental results and the middle and lower curves are, respectively, results calculated for $G = 2 - |\Delta|$ and 1.75. The vertical lines are calculated oscillator strengths for dipole-allowed transitions to or from the MO levels. Vacuum level is indicated by VL.

and Cl $K\beta$ emission spectra exhibit, respectively, a shoulder and a dip at the high-energy sides of the respective main peaks. These structures are due to the effect of self-absorption of the emitted x ray in the spectral region overlapping with the absorption region. With respect to absorption spectra, the observed Cl K absorption spectrum shows more complicated structures as compared with the observed Pd L_{III} absorption spectrum. We will make comments on this at the end of this section.

The calculated spectra are presented at lower parts in Figs. 6 and 7, where vertical lines denote calculated oscillator strengths for dipole-allowed transitions to or from MO's, and solid and dashed curves are the spectra broadened by Lorentzian curves. The value of a parameter for the Lorentzian broadening was determined as 3.75 eV for Pd spectra and 2.5 eV for Cl spectra from fitting for the widths of the first peaks of Pd L_{III} and Cl K absorption spectra. We assumed that the parameter for emission is the same as that for absorption for simplicity.

We are now in a position to discuss our results, making a comparison of experimental and theoretical results. First, let us confine ourselves to discussion of the emission spectra and the first peak of the absorption spectra. The energy separation (ΔE) between the main peak of the emission spectrum and the first peak of the absorption spectrum is one of good objects of the present discus-

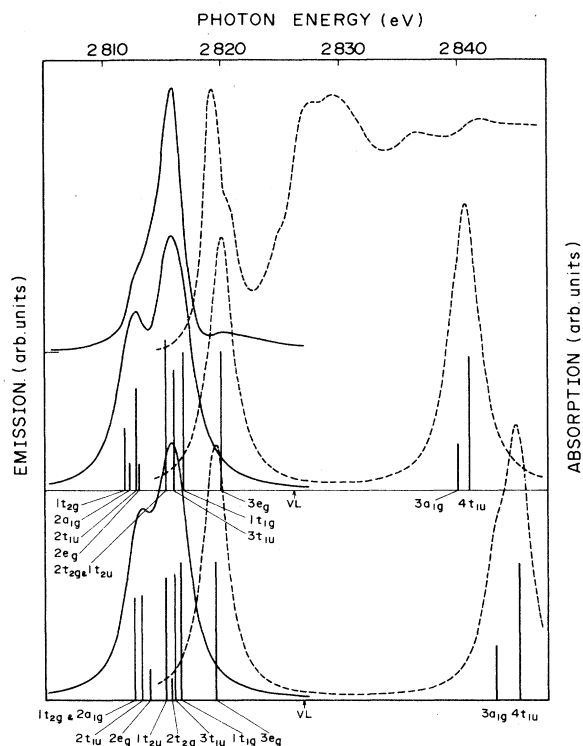


FIG. 7. Cl $K\beta$ emission (solid curves) and Cl K absorption (dashed curves) spectra. Upper curves are the experimental results. Middle and lower curves are calculated results for $G=2-|\Delta|$ and 1.75, respectively. The vertical lines are calculated oscillator strengths for dipole-allowed transitions.

sion. The values of ΔE obtained experimentally in the Pd and Cl spectra differ from each other, being 4.75 eV for the Pd spectra and 3.3 eV for the Cl spectra. From the calculated spectra the former is determined to be 5.0 eV for $G=2-|\Delta|$ and 3.9 eV for $G=1.75$; the latter is determined to be 4.25 eV for $G=2-|\Delta|$ and 3.6 eV for $G=1.75$. The agreement between experiment and calculation is satisfactory. The observed difference of ΔE between the Pd and Cl spectra is, as can be seen from Figs. 6 and 7, a direct reflection of the existence of two MO ($3t_{1u}$ and $1t_{1g}$) levels between $2t_{2g}$ and $3e_g$ whose separation determines the value of $10Dq$. The spectral profiles of the calculated Cl spectra considerably reproduce the features observed experimentally, except for a small shoulder appearing at the high-energy side of the first peak of the absorption. In the case of Pd spectra, however, the asymmetry of the emission spectrum is opposite to each other; that is, the experimental spectrum is asymmetrically broadened at the high-energy side, while the calculated one is asymmetrically broadened at the low-energy side. The disagreement for the asymmetry of the Pd $L\beta_{2,15}$ emission spectrum would not be improved unless a drastic change occurs in order of MO levels. If we accept such discrepancies, the spectral features observed experimentally in the overlapping regions of the emission and absorption are generally explained by our calculation

based on the self-consistent-charge extended Hückel method. Here, we should comment on the adjustable parameter G . We have seen that the calculated results depend on a choice of the parameter G . From our results presented here, however, we cannot judge which choice is better.

Next, we discuss the peak which follows the first peak in the absorption spectrum. The peak of the calculated spectrum corresponding to the transitions to $3a_{1g}$ and $4t_{1u}$ MO's is largely separated from the first peak, contrary to the experimental result, which shows that the second peak appears about 10 eV above the first peak in both the spectra. This seems to suggest the limitation of the MO calculation, which takes into account only a definite small number of atomic orbitals. This situation is very similar to that encountered in the problem of energy-band calculations by a linear combination of atomic orbitals (LCAO) method,³⁰ which leads to good valence bands, but does not necessarily lead to good conduction bands. Furthermore, the peaks following the first peak do not have the nature of bound-to-bound transitions, but instead are associated with transitions to continuum states. Therefore, the multiple-scattering theory mentioned in the Introduction is used to describe the absorption in this energy region. We make a remark on the different features observed in Pd and Cl absorption spectra in connection with the multiple-scattering theory. According to this theory,¹³ it is readily understood that the complication of absorption spectra is closely related to the geometrical arrangement of atoms around the x-ray-absorbing atom. In K_2PdCl_6 crystal, as seen from Fig. 1, the Pd ion is octahedrally surrounded by six Cl ions, while the Cl ion is surrounded by a few kinds of ions in a more complicated manner. This seems to be the main reason why the Cl K absorption spectrum exhibits complicated structures as compared with the Pd L_{III} absorption spectrum. Unfortunately, the crystal structure is too complicated to perform the multiple-scattering calculation for K_2PdCl_6 .

Finally, we would like to mention the effect of a core hole created in the absorption process. We have considered this effect for Pd spectra using the concept of the transition states,¹⁴ in which half an electron is removed from the core orbital in the Pd metal at the center of the MX_6 cluster. In the case of Pd spectra, the same calculations as those described above could be easily done without modifying the formulation, because O_h symmetry is retained. The result in this case was found to be almost the same as those shown above, with respect to both the spectral shape and energy separation ΔE .

V. SUMMARY

We have measured Pd $L\beta_{2,15}$ and Cl $K\beta$ emission spectra for a K_2PdCl_6 crystal and interpreted their results and Pd L_{III} and Cl K absorption spectra reported previously,^{10,11} in terms of the molecular-orbital calculations based on the self-consistent-charge extended Hückel method.

Our main results are as follows.

(1) The spectral features observed experimentally in the overlapping regions of the emission and absorption spectra are fairly well explained by our calculations.

(2) The experimental energy separation between the main peak of the emission spectrum and the first peak of the absorption spectrum is 4.75 eV for Pd spectra and 3.3

eV for Cl spectra.

This difference is shown to be a direct reflection of the existence of two molecular-orbital levels ($3t_{1u}$ and $1t_{1g}$) between $2t_{2g}$ and $3e_g$ levels whose energy separation determines the value of $10Dq$.

- ¹S. Sugano and R. G. Shulman, *Phys. Rev.* **130**, 517 (1963).
²C. J. Ballhausen and H. B. Gray, *Molecular Orbital Theory* (Benjamin, New York, 1965).
³B. Kleinman and M. Karplus, *Phys. Rev. B* **3**, 24 (1971).
⁴T. F. Soules, J. W. Richardson, and D. M. Vaught, *Phys. Rev. B* **3**, 2186 (1971).
⁵T. F. Soules, E. J. Kelly, and D. M. Vaught, *Phys. Rev. B* **6**, 1519 (1972).
⁶H. Terasawa, T. Kambara, K. I. Gondaira, T. Teranishi, and K. Sato, *J. Phys. C* **13**, 5615 (1980).
⁷S. Sakoda and T. Tsuboi, *Phys. Rev. B* **22**, 4966 (1980).
⁸S. Larsson, J. S. Tse, J. L. Esquivel, and A. Tangkai, *Chem. Phys.* **89**, 43 (1984).
⁹S. Larsson and P. Pyykkö, *Chem. Phys.* **101**, 355 (1986).
¹⁰C. Sugiura and M. Ohashi, *J. Chem. Phys.* **78**, 88 (1983).
¹¹C. Sugiura and S. Muramatsu, *J. Chem. Phys.* **82**, 2191 (1985).
¹²D. W. Fischer, *J. Phys. Chem. Solids* **32**, 2455 (1971); in *Band Structure Spectroscopy of Metals and Alloys*, edited by D. J. Fabian and L. M. Watson (Academic, London, 1973); *Phys. Rev. B* **5**, 4219 (1972); **8**, 3576 (1973).
¹³M. Kitamura, S. Muramatsu, and C. Sugiura, *Phys. Rev. B* **33**, 5294 (1986).
¹⁴M. Kitamura, C. Sugiura, and S. Muramatsu, *Solid State Commun.* **62**, 663 (1987).
¹⁵M. Kitamura, S. Muramatsu, and C. Sugiura, *Phys. Status Solidi B* **142**, 191 (1987).
¹⁶M. Kitamura, S. Muramatsu, and C. Sugiura, *Phys. Rev. B* **37**, 6486 (1988).
¹⁷M. Kitamura, C. Sugiura, and S. Muramatsu, *Solid State Commun.* **67**, 313 (1988).
¹⁸M. Kitamura, C. Sugiura, and S. Muramatsu, *Phys. Status Solidi B* **149**, 791 (1988).
¹⁹R. W. G. Wyckoff, *Crystal Structures* (Interscience, New York, 1951), Vol. 3.
²⁰C. Sugiura, M. Kitamura, S. Muramatsu, S. Shoji, S. Kojima, Y. Tada, I. Umezumi, and T. Arai, *Jpn. J. Appl. Phys.* **27**, 1216 (1988).
²¹J. A. Bearden, *Rev. Mod. Phys.* **39**, 78 (1967).
²²J. Valasek, *Phys. Rev.* **53**, 274 (1938).
²³H. M. Evjen, *Phys. Rev.* **39**, 675 (1932).
²⁴M. Wolfsberg and L. Helmholz, *J. Chem. Phys.* **20**, 837 (1962).
²⁵J. C. Slater and G. F. Koster, *Phys. Rev.* **94**, 1498 (1954).
²⁶M. Kitamura, S. Muramatsu, and C. Sugiura, *Phys. Rev. A* **35**, 2838 (1987).
²⁷R. Manne and T. Åberg, *Chem. Phys. Lett.* **7**, 282 (1970).
²⁸F. Herman and S. Skillman, *Atomic Structure Calculations* (Prentice-Hall, Englewood Cliffs, NJ, 1963).
²⁹K. Schwarz, *Phys. Rev. B* **5**, 2466 (1972).
³⁰W. A. Harrison, *Electronic Structure and the Properties of Solids, The Physics of the Chemical Bond* (Freeman, San Francisco, 1980).
³¹L. C. Cusachs, *J. Chem. Phys.* **43**, S157 (1965).
³²N. V. Bhat, *Spectrochim. Acta* **28B**, 257 (1973).
³³C. K. Jørgensen, *Absorption Spectra and Chemical Bonding in Complexes* (Pergamon, London, 1962).